Journal of Innovative Optical Health Sciences
Vol. 2, No. 3 (2009) 235–244

World Scientific
www.worldscientific.com

EFFECTS OF SPECTRAL DEPENDENCE IN PASS-THROUGH PHOTON-BASED BIOMEDICAL TRANSILLUMINATION

PAULINO VACAS-JACQUES*, MARIJA STROJNIK
and GONZALO PAEZ
Centro de Investigaciones en Optica, Apartado Postal 1-948
37000, Leon, Guanajuato, Mexico
**pvj@cio.mx*

We have proposed an interferometric setup for biomedical analysis in transillumination modality. Wavelength dependence of optical properties must be considered for selecting source and sample. An expansion of the sample optical properties, around the central wavelength of emission, serves to account for spectral effects. Expected spectral values depend on the central moments of the source, and specific constants associated to the optical properties of the sample. By matching wavelength characteristics of source and sample, a first-order approximation is applicable. In such case, the expected values are exactly the optical properties evaluated at the central wavelength. Furthermore, in the first-order approximation, the transillumination interferometer yields the integrated attenuation of the sample at the central wavelength of emission. We verify the latter assertion by performing a wavelength-dependent Monte Carlo analysis to calculate the response of the transillumination interferometer. Recovered attenuation coefficients, for imaging and characterization scenarios, are in agreement with the value computed at the central wavelength of the source.

Keywords: Transillumination; wavelength-dependent Monte Carlo; tissue characterization; tissue imaging.

1. Introduction

The challenge of preventing and reducing dental caries remains a significant endeavor. In the United States, approximately 20% of children have detectable caries. Almost 80% of young people have had a cavity, and 66% of adults have lost at least one permanent tooth due to dental caries.[1] Detection of incipient and hidden lesions is required to prevent and reduce caries.[2] Therefore, the identification of early dental decay is a current research topic of interest. An important reason for undertaking such investigations is that treatment of patients, with nonsurgical methods, is readily performed. Moreover, objective methods for diagnosis are a central component to enable preventive intervention.

In our group, we are interested in addressing the identification and characterization of early dental decay. Furthermore, the method we have proposed employs pass-through or ballistic photons in an interferometer. The use of ballistic photons renders the technique especially sensitive to variations in sample extent and composition. High sensitivity may be particularly relevant for longitudinal screening. By isolating the changes in morphology, we may concentrate on the alterations in tissue (i.e., enamel)

*Corresponding author.

structure. The importance of identifying variations in enamel structure concerns the detection of incipient lesions. Early development of caries is characterized by a demineralization process, which modifies enamel structure.[3,4] Thus, a diagnostic method with sensitivity to changes in enamel structure may provide a means to detect earlier dental decay.

Previously, we described the response of the ballistic transillumination interferometer, when using laser light.[5–8] We complemented such analysis by considering the effects of forward-scattered radiation.[9] For this purpose, a monochromatic Monte Carlo (MC) study of dental enamel was performed.[10] Forward-scattered and pass-through contributions were shown to be comingled.[11] We, therefore, implemented a partial-coherence transillumination setup to assess enamel-like samples with ballistic photons.[12] Recently, by employing the monochromatic MC approach, we have described the theoretical response of the partial-coherence interferometer. In addition, we discussed the feasibility of evaluating early dental decay with the technique.[13]

In this work, we describe the effects of spectral dependence in the transillumination interferometer. We demonstrate theoretically that the technique yields the integrated attenuation of the sample at the central wavelength of emission. This result, nevertheless, depends on the selection of an adequate radiation source for performing the analysis. The emission spectrum of the source should be confined to a wavelength interval, where the optical properties of the sample do not vary abruptly.

In the following section, we extend the theoretical model of pass-through photon-based biomedical transillumination. For this purpose, we describe the implementation of a wavelength-dependent MC analysis to calculate the response of the technique. In Sec. 3 of this work, we introduce the spectral tissue model. The response of the interferometer is then addressed in Sec. 4. Finally, in Sec. 5, we conclude and present future research directions.

2. Theory

2.1. *Wavelength-dependent pass-through transillumination*

In pass-through photon-based biomedical transillumination, we employ ballistic photons and interference to probe the sample. In Fig. 1, we depict a schematic of the technique, while highlighting wavelength-dependent features.

The medium under test is located in one arm of the interferometer, whereas a reference delay line is in the other. Radiation with a determined bandwidth impinges on the sample. Thereafter, multiple random walks of photons throughout the turbid medium take place. The distribution of transmitted photons retains the signature of the spectral characteristics of the sample. In particular, the pass-through field is related to the incident one as given by the following expression.[8,12]

$$\mathbf{E}_{\mathrm{p}} = \left[R_g \exp\left(-i\frac{2\pi}{\lambda} 2 n_g(\lambda) d \right) \cdot \exp\left(\sum_i -\frac{1}{2}(\mu_{a_i}(\lambda) + \mu_{s_i}(\lambda)) D_i \right) \cdot \exp\left(-i\frac{2\pi}{\lambda} \sum_i n_{s_i}(\lambda) D_i \right) \right] \mathbf{E}_{\mathrm{s}}. \quad (1)$$

Here, $\mathbf{E}_{\mathrm{p}}$ and $\mathbf{E}_{\mathrm{s}}$ refer to pass-through and incident (i.e., sample) fields. Quantities written using bold letters are complex. R_g is the Fresnel reflection coefficient. λ stands for wavelength. The refractive index and thickness of the container, for *in vitro* studies, are n_g and d. The ith absorption and scattering coefficients of the sample are described by μ_{a_i}

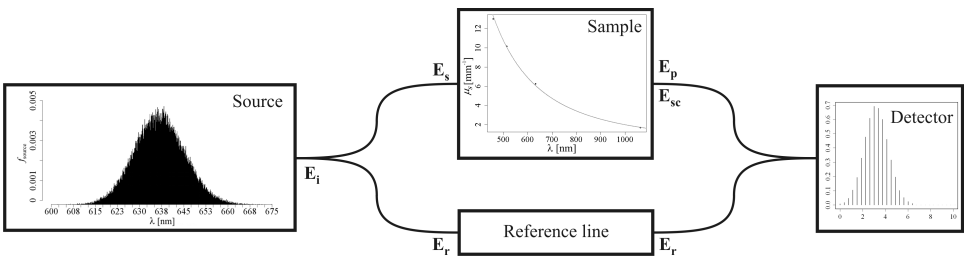

Fig. 1. In pass-through photon-based transillumination, radiation with a specific bandwidth impinges on the sample, located in one arm of the interferometer. Coherent superposition is used to recover the information of interest. Incident $\mathbf{E}_{\mathrm{i}}$, sample $\mathbf{E}_{\mathrm{s}}$, reference $\mathbf{E}_{\mathrm{r}}$, pass-through $\mathbf{E}_{\mathrm{p}}$, and forward-scattered $\mathbf{E}_{\mathrm{sc}}$ electrical fields are shown explicitly.

and μ_{s_i}. Meanwhile, the associated sample thickness and refractive index are D_i and n_{s_i}. The term in square brackets has been variously named as material coherence function and transmission profile function.[5–8]

In Eq. (1), the wavelength dependence of the optical properties of the sample is explicitly taken into consideration. The direction of scattering, frequently described by the anisotropy factor g, is also a function of wavelength. To further understand the spectral effects, we describe the optical properties in terms of wavelength or, alternatively, optical frequency. For this purpose, we perform an expansion of the optical properties around the central wavelength, $\bar{\lambda}$.

$$\mu_s(\lambda) = \mu_s(\bar{\lambda}) + (\lambda - \bar{\lambda})\left.\frac{d\mu_s(\lambda)}{d\lambda}\right|_{\bar{\lambda}} + \frac{(\lambda-\bar{\lambda})^2}{2!}\left.\frac{d^2\mu_s(\lambda)}{d\lambda^2}\right|_{\bar{\lambda}} + \frac{(\lambda-\bar{\lambda})^3}{3!}\left.\frac{d^3\mu_s(\lambda)}{d\lambda^3}\right|_{\bar{\lambda}} + \cdots \quad [\mathrm{mm}^{-1}]. \tag{2}$$

For brevity in Eq. (2), we present exclusively the relation for the scattering coefficient. However, similar expressions are implied for the remaining optical properties. For inverse-wavelength dependence, the expansion may be performed in terms of the optical frequency.

The wavelength of emission is randomly distributed. Therefore, an instantaneous realization of the optical properties, as described in Eq. (2), is of modest relevance. In contrast, the assessment of the statistical expectation provides more significant information.

$$E\{\mu_s(\lambda)\} = \sum_k \frac{m_k}{k!}\left.\frac{d^k\mu_s(\lambda)}{d\lambda^k}\right|_{\bar{\lambda}} \quad [\mathrm{mm}^{-1}]. \tag{3}$$

Here, $E\{\,\}$ denotes statistical expectation, and m_k stands for the kth central moment of the distribution. From Eq. (3), we ascertain that expected spectral values depend on the central moments of the source, and specific constants associated to the optical properties of the sample. A relevant scenario occurs in the first-order approximation. For such cases $E\{\mu_s(\lambda)\} = \mu_s(\bar{\lambda})$, because the first central moment is by definition zero. We should point out that this result is general, because it is independent of the expansion variable and of the distribution function. Thus in the first-order approximation, the expected values are given by the optical properties evaluated at the central wavelength.

Equation (3) implies that a match between the optical properties of the sample and the radiation source is important. For the transillumination interferometer, this tradeoff is a relevant feature. Take, for example, a sample with a strong absorption peak in the interval of interest. Then, the first-order approximation would only be valid if the second moment of the source is near zero. On the other hand, if the sample does not exhibit abrupt changes in the optical properties, the value of the second moment is of minor importance. Thus, we may describe an optimal match between the spectral characteristics of source and sample. This configuration ensues when the emission spectrum of the source is confined to a wavelength interval, where the optical properties of the sample do not vary abruptly. In such scenario, the first-order approximation in Eq. (3) applies, and Eq. (1) is modified accordingly.

$$\mathbf{E}_\mathrm{p} = \left[R_g \exp\left(-i\frac{2\pi}{\bar{\lambda}}2n_g(\bar{\lambda})d\right) \cdot \exp\left(\sum_i -\frac{1}{2}(\mu_{a_i}(\bar{\lambda}) + \mu_{s_i}(\bar{\lambda}))D_i\right) \cdot \exp\left(-i\frac{2\pi}{\bar{\lambda}}\sum_i n_{s_i}(\bar{\lambda})D_i\right)\right]\mathbf{E}_\mathrm{s}. \tag{4}$$

The expression in Eq. (4) implies that the transillumination interferometer yields the integrated attenuation of the sample at the central wavelength of emission. The assertion is true, provided that spectral characteristics of source and sample match.

2.2. *Interferometer response and wavelength-dependent MC analysis*

In a recent publication, we described in detail the theoretical behavior of the transillumination technique.[13] We may calculate the interferometer response by resorting to the theory of low-coherence optical tomography.[14,15] The power collected by the detector is found by superposing sample $\mathbf{E}_\mathrm{s}$ and reference $\mathbf{E}_\mathrm{r}$ beams (see Fig. 1).

$$P(\Delta L/c) = \left\langle \left[\int_{-\infty}^{\infty} \mathbf{E}'_\mathrm{s}(\tau, L_s)dL_s + \mathbf{E}_\mathrm{r}(\tau + t)\right] \cdot \left[\int_{-\infty}^{\infty} \mathbf{E}'_\mathrm{s}(\tau, L_s)dL_s + \mathbf{E}_\mathrm{r}(\tau + t)\right]^* \right\rangle \quad [\mathrm{W}]. \tag{5}$$

Here, P represents the detected power. $\Delta L = L_r - L_s$ is the optical path-length difference. L_r and L_s stand for optical path-lengths of reference and sample arms. c is the velocity of light in vacuum. τ is the reference time for partial-coherence modeling, and t represents modulation time. $\mathbf{E}'(\tau, L_s)$ is defined as the path-length-resolved field density; $\mathbf{E}'(\tau, L_s) = \partial\mathbf{E}(\tau, L_s)/\partial L_s$. The chevrons denote time average and an asterisk demarcates complex conjugation.

Sample path-lengths do not depend on the reference scan delay. Therefore, we may express Eq. (5) in an alternative form.

$$P(L_r) = 2(P_r P_s)^{1/2} \int_{-\infty}^{\infty} [T(L_s)]^{1/2} |\gamma_{i,i}(\Delta L)| \times \cos[\Phi_{i,i}(\Delta L)] dL_s \ \ [\mathrm{W}]. \tag{6}$$

In Eq. (6), we evaluate exclusively the modulated terms of Eq. (5). Reference and sample dc contributions are P_r and P_s. In addition, $|\gamma_{i,i}|$ and $\Phi_{i,i}$ represent amplitude and phase of the complex degree of self-coherence. Finally, $T(L_s)$ stands for path-length-resolved transmittance; $T(L_s) = [\mathrm{d}P_s(L_s)/\mathrm{d}L_s]/P_s$. In reflection geometries, such as those used in optical coherence tomography, $T(L_s)$ is replaced by the path-length-resolved reflectance.[14,15]

The response of the interferometer is given by the convolution of Eq. (6). From linear systems theory, the behavior of the technique is calculated by passing the path-length-resolved transmittance through a filter. The shape of the filter is determined by the power spectrum of the source. For sources used in partial-coherence interferometry, filters are centered at high frequencies and have narrow bandwidths.[13–15] Hence, the technique is mainly sensitive to the fast-varying components of $[T(L_s)]^{1/2}$. Pass-through radiation is an ideal high-frequency component of sample transmittance. Thus, the transillumination interferometer is particularly useful for detecting ballistic photons.

The path-length-resolved transmittance depends on the optical properties of the sample. The optical properties are, in turn, a function of wavelength. In order to determine path-length-resolved transmittances, considering wavelength dependence, we perform random walk MC calculations.

In the MC analysis, we implement additional features as compared to those of traditional approaches.[14,16,17] First, we incorporate diverse power spectral densities. These include radiation sources with Gaussian, uniform, and Lorentzian spectra. The required data for computing power spectra consist of the half-power bandwidth and the central wavelength. Random variates are calculated in the optical frequency domain. However, they are stored as wavelength values for future use. Second, we include several models to fit the optical properties of the sample. Linear, power, polynomial, exponential, and cubic spline models may be employed. The resulting functions, which predict the values of the optical properties, are calculated in R.[18] We allocate to each medium a prediction function for further processing.

In traditional MC implementations, the radiation impinging on the turbid medium is monochromatic. Therefore, in the generation of packet of photons no spectral considerations are needed. In the application of interest, in contrast, the radiation has a bandwidth. Thus, in the procedure for generating a packet of photons, the spectral characteristics of source and turbid medium are required. We sample the power spectral density of the source to determine the wavelength of the packet of photons. Thereafter, we update the optical properties of the media using wavelength information and prediction functions. The values of the optical properties remain the same for the complete random walk of a packet of photons. Next, we launch and propagate the packet of photons according to the rules of traditional MC implementations.

From the wavelength-dependent MC analysis, we compute the path-length-resolved transmittance. Afterward, we convolve the path-length-resolved transmittance with the coherence characteristics of the source, as shown in Eq. (6). Then, we recover the information of interest by finding the maxima of the interferograms. We normalize maxima values to account for interferometer features, including container effects. Finally, we take the logarithm of the normalized values to retrieve the integrated attenuation of the sample. Further details regarding the recovery of information are available in the literature.[12,13]

3. Spectral Tissue Model

The main objective of the present work is to describe the spectral behavior of the ballistic transillumination interferometer. In addition to this principal motivation, we seek to eliminate sources of error in our system, and we look for continuity in our research. In order to minimize errors, we attend

to a particular scenario where deviations from theory have been observed in the experiment.[12] For the sake of continuity, in this work, the setting (i.e., radiation source, holder, and sample) is similar to the one encountered in the experimental validation of the technique. The radiation source is an LED with emission in the red portion of the spectrum. The radiation impinges on a 1 mm thick cuvette, which holds the sample. The latter is a lipid-based emulsion, in accordance with the experiment. More specifically, the sample we use is Intralipid-10%; the turbid medium employed as reference to validate the experiment.[12]

The spectral characteristics of Intralipid-10% are well described in the literature.[19] In addition, the behavior of the scattering coefficient as a function of concentration has been reported.[20] In Fig. 2, we present the spectral characteristics of the scattering coefficient for various concentrations. The behavior in (a) is representative of a sample with no dilution. For (b) and (c), we consider the Intralipid-10% to be diluted in water to: 1 part in 10 for (b), and 1 part in 8 for (c).

Before pursuing the description of the sample, we draw a parallel between the optical properties of Intralipid-10% and those of enamel. Sound dental enamel exhibits a remarkable transparency to radiation centered at 1310 nm.[21] At this wavelength range, the attenuation coefficient of sound enamel $\mu_t = \mu_a + \mu_s$ is roughly $0.4\,\mathrm{mm}^{-1}$, and does not change abruptly.[22]

The decay of ballistic radiation is not governed uniquely by the attenuation coefficient. Rather it is the optical depth, which describes the attenuation strength of a sample. The optical depth is simply attenuation coefficient [mm^{-1}] multiplied by sample distance [mm]. Hence, a 10 mm sample of sound enamel, at 1310 nm, exhibits an optical depth of 4. Even though in the current work we do not focus explicitly on enamel, we equate the optical depths of Intralipid-10% and enamel.

In the red portion of the spectrum, the behavior in Fig. 2(b) resembles the attenuation of sound enamel. Meanwhile, the characteristics in Fig. 2(c) exhibit a greater attenuation. Such a tendency is distinctive of demineralized enamel.[3,22] For this study, we attend to the case of greater lipid-concentration, i.e., Fig. 2(c). In the experiment, we observed deviations from theory in such scenarios. We are, therefore, interested in gaining

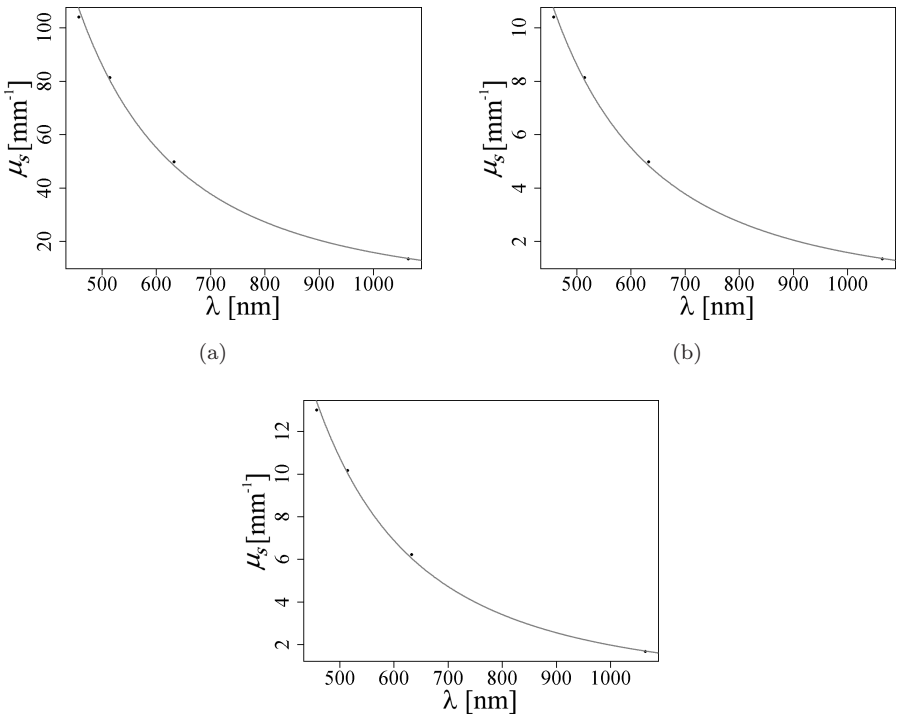

Fig. 2. Scattering coefficient of Intralipid-10% as concentration varies. The behavior in (a) is representative of a sample with no dilution.[19] For (b) and (c), we consider the Intralipid-10% to be diluted in water to: 1 part in 10 for (b), and 1 part in 8 for (c).

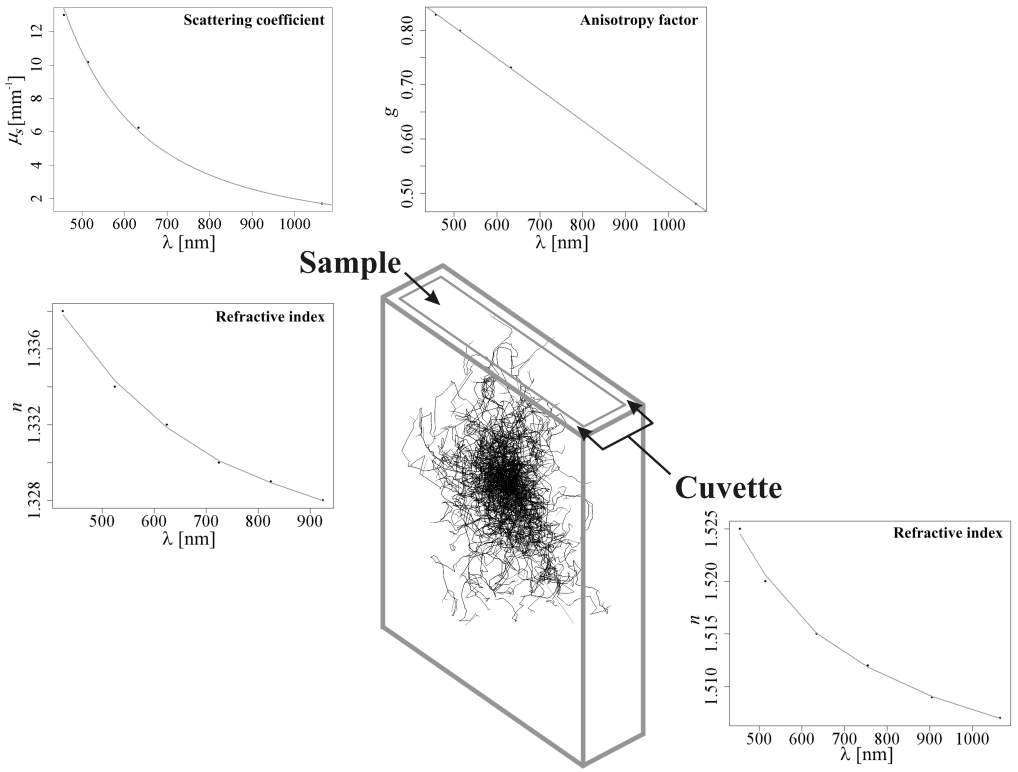

Fig. 3. The spectral tissue model consists of a container and Intralipid-10%. Values of refractive index versus wavelength are those of BK7 glass (cuvette) and water (sample). The scattering coefficient of the turbid medium corresponds to that of Fig. 2(c). The spectral dependence of the anisotropy is taken from the literature.[19]

further insight with respect to the origins of the discrepancies.

In order to complete the description of the tissue model, we recall that the turbid medium is contained in a 1 mm glass cuvette. The latter is surrounded by air. In Fig. 3, we present the spectral tissue model under consideration. We depict explicitly the wavelength dependence of the optical properties. In addition, we note that only few data points are required to construct the spectral tissue model. Furthermore, fit functions span a broad range of wavelengths.

The cuvette is made of BK7 glass. The spectral dependence of the refractive index, for BK7 glass, is readily at hand.[23] For the turbid medium, the values of refractive index and wavelength are those of water.[24] Fit functions of the refractive indices are splines. Absorption properties are considered to be negligible, and thus not shown in Fig. 3. Sample scattering characteristics are described by power and linear fit functions. The former behavior is distinctive of the scattering coefficient, whereas the latter is representative of the anisotropy factor.[25] Finally, we note that the Henyey–Greenstein phase function is used in the MC analysis.

4. Effects of Spectral Dependence in the Interferometer Response

We perform the wavelength-dependent MC analysis for two scenarios, tissue characterization and imaging. The basic difference between both is the spatial extent of the beam. For the former application the beam diameter is 0.5 mm, whereas for the latter it is 15-fold greater. In each case, the spatial distribution is flat-field and the beam is collimated.

We assess a partially coherent source with Gaussian spectrum. As in the experiment, the assessed central wavelength is 637 nm, and the bandwidth equals 20 nm.[12] After performing the MC analysis, we obtain the power density of the source. The latter is shown in Fig. 4 for the case of tissue characterization.

From the MC results of Fig. 4, we recognize that the optical properties of the sample (see Fig. 3) should be restricted to the range $[\bar{\lambda} - \Delta\lambda, \bar{\lambda} + \Delta\lambda]$.

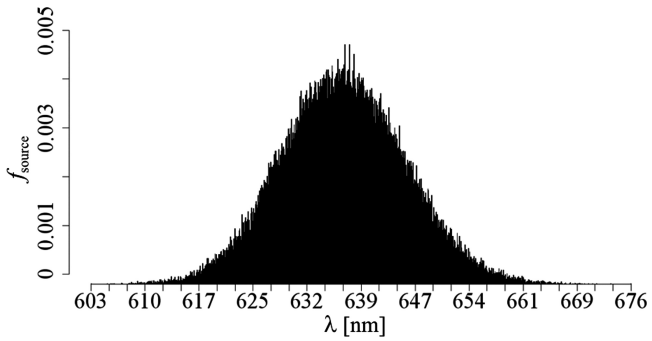

Fig. 4. We perform a wavelength-dependent Monte Carlo (MC) analysis to describe the interactions between radiation and sample. After MC calculations, we obtain the resulting emission of the source.

In Fig. 5, we confine the optical properties of the sample to be within these limits.

The information shown in Fig. 5 is relevant for the application being discussed. We ascertain that the optical properties behave linearly in the spectral range of interest. Thus, the transillumination interferometer should yield the integrated attenuation of the sample assessed at the central wavelength. We determine the reference attenuation from the plot of the scattering coefficient. For a central wavelength of 637 nm, the reference coefficient is $5.955\,\mathrm{mm}^{-1}$.

The wavelength-dependent MC analysis enables the calculation of path-length-resolved transmittances. Thereafter, we convolve such information with the function describing the coherence characteristics of the source. From such calculations, we obtain the spectral response of the transillumination interferometer. Finally, by finding the maxima of the interferograms, we recover the information of the integrated attenuation of the sample.

In Fig. 6, we show the path-length-resolved transmittances for both scenarios. To construct the plots, we subtract the least path-length traversed by transmitted photons. We concentrate exclusively on the effects of spectral dependence in the transillumination interferometer. In the figure, plots in (a) refer to the characterization scenario. Meanwhile, those corresponding to imaging are shown in (b). In turn, the plots in (c) are the response of the reference setup (i.e., one without attenuating centers). Each of these representations describes the traversal of ballistic photons through the sample. Additionally, in each plot, we have excluded the effects of forward scattering. We refer the reader to a recent publication, where we discuss the contributions of such radiation.[13]

Multiple peaks in the plots of path-length-resolved transmittance are due to Fresnel reflections. These are accounted for in the MC analysis. Furthermore, in the inset of each representation, we illustrate in more detail the effects of spectral dependence. Broadening of the delta-like signature of ballistic photons is readily ascertained. With this information, we proceed to recover the integrated attenuation of the sample. We convolve path-length-resolved information with coherence characteristics of the source, and find the maxima for sample and reference scenarios.

In the case under study, the integrated attenuation actually yields the attenuation coefficient. This assertion is true, because the sample is composed solely of one layer (1 mm thick). The recovered values of integrated attenuation, for characterization and imaging, read 5.840 and $5.947\,\mathrm{mm}^{-1}$. Recovered coefficients are in good agreement with the value computed at the central wavelength of the source, $5.955\,\mathrm{mm}^{-1}$ (see Fig. 5). We attribute the variations to the exponential attenuation of ballistic photons. In the MC analysis, we ascertained a difference of 5% in the number of pass-through photons between scenarios. Unmistakably, more ballistic photons traversed the sample in tissue characterization simulations. A direct means to reduce

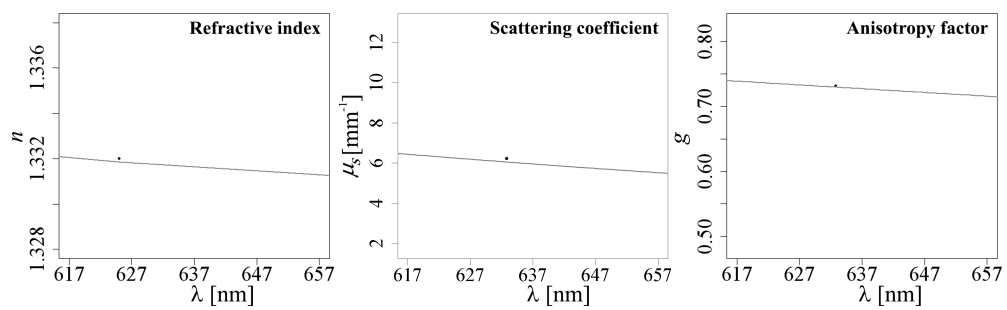

Fig. 5. The optical properties behave linearly in the spectral range of interest. The reference attenuation may be computed from the representation of the scattering coefficient, using the value of the central wavelength.

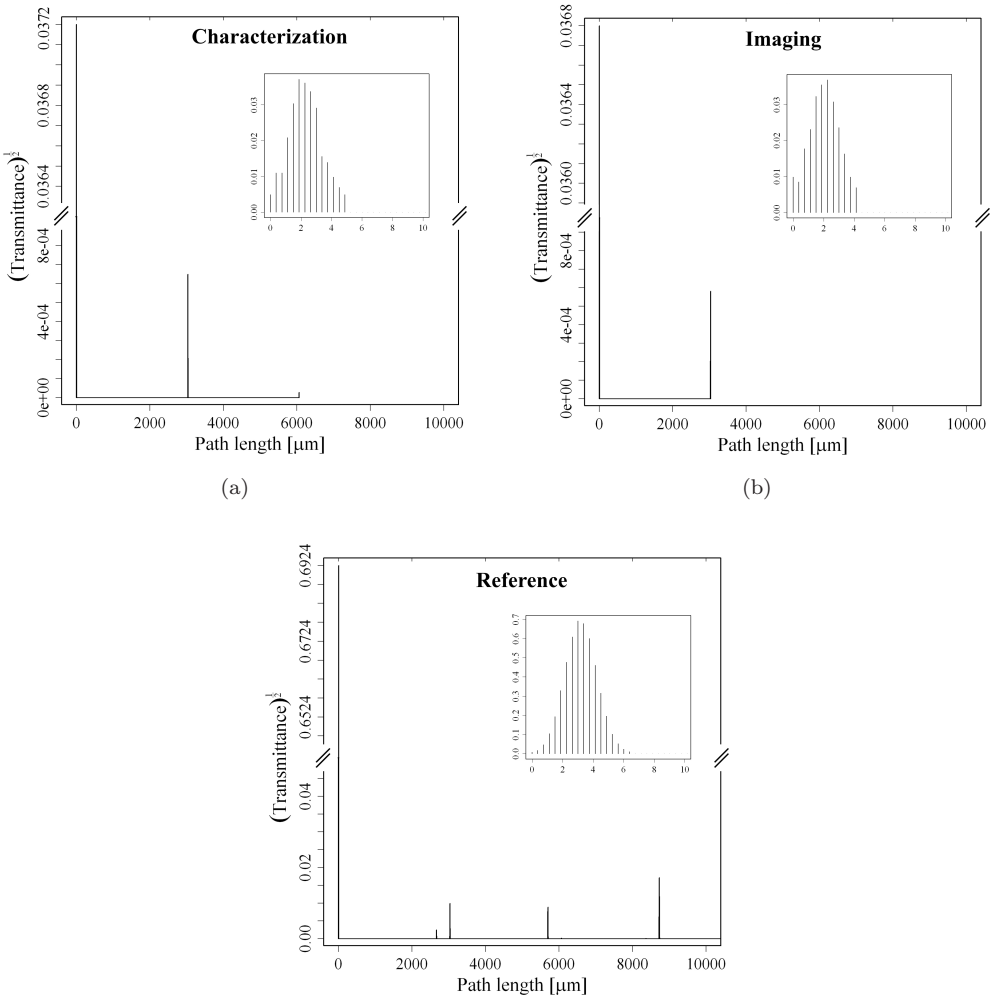

Fig. 6. Path-length-resolved transmittances for (a) characterization, (b) imaging, and (c) reference scenarios. In each inset, we illustrate in more detail the first transmittance peak.

these deviations is to increase the number of photons in MC calculations.

Variations in the recovered attenuation, due to spectral effects, have an additional implication. The deviations are not significant enough to account for the discrepancies observed experimentally. Thus, as a result of this work, we suggest to improve the detection scheme of the experiment. A plausible approach could entail the implementation of balanced detection.

5. Conclusions and Future Work

We have addressed the effects of spectral dependence in pass-through photon-based biomedical transillumination. In the analysis, we proposed an expansion of the optical properties of the sample, around the central wavelength of emission of the source. Expected spectral values depend on the central moments of the source, and specific constants related to the optical properties of the sample. In the first-order approximation, expected values are exactly the optical properties evaluated at the central wavelength. This assertion is true, provided that spectral characteristics of source and sample correspond. An optimal match ensues when the emission spectrum of the source is confined to a wavelength interval, where the optical properties of the sample do not vary abruptly.

We described, and implemented, a wavelength-dependent MC analysis to calculate the response of the transillumination interferometer. Additional required parameters, as compared to traditional MC calculations, are power density and spectral optical properties. From the stochastic analysis, we obtained the path-length-resolved transmittance,

and ascertained the effects of spectral dependence. Finally, we showed that the recovered information was in good agreement with the value computed at the central wavelength of the source.

We thus conclude that, the transillumination interferometer yields the integrated attenuation of the sample at the central wavelength, provided that spectral characteristics of source and sample match.

A future research direction is the improvement of the detection phase of the experiment. A plausible approach would entail the implementation of a balanced interferometer.

Acknowledgments

Paulino Vacas-Jacques gratefully acknowledges the National Science and Technology Council of Mexico (CONACyT) for the financial support assigned to participate at Saratov State University, grant 172068. The same author thanks the "Centro de Investigaciones en Optica" for partial funding of travel expenses.

This research was performed in the framework of the project "Applications of infrared interferometry for biomedical tomography" (CONACyT 2007-I0003-60450).

References

1. Diagnosis and management of dental caries throughout life, National Institutes of Health Consensus Statement **18**, 1–30 (2001).
2. D. Boston, "Incipient and hidden caries," *Dent. Clin. N. Am.* **49**, xi–xii (2005).
3. C. Darling, G. Huynh, D. Fried, "Light scattering properties of natural and artificially demineralized dental enamel at 1310 nm," *J. Biomed. Opt.* **11**, 034023 (2006).
4. I. Pretty, "Caries detection and diagnosis: Novel technologies," *J. Dent.* **34**, 727–739 (2006).
5. G. Paez, M. Strojnik, M. Scholl, "Interferometric tissue characterization: I. Theory," in *Infrared Spaceborne Remote Sensing 2005*, M. Strojnik, ed., Proc. SPIE 5883, Bellingham, 58830Y (2005).
6. M. Strojnik, G. Paez, "Interferometric tissue characterization: II. Experimental," in *Infrared Spaceborne Remote Sensing 2005*, M. Strojnik, ed., Proc. SPIE 5883, Bellingham, 58830W (2005).
7. M. Strojnik, G. Paez, "Interferometric tissue characterization: III. Calibration," in *Infrared Spaceborne Remote Sensing 2005*, M. Strojnik, ed., Proc. SPIE 5883, Bellingham, 58830V (2005).
8. G. Paez, M. Strojnik, S. Scholl, "Interferometric tissue characterization: IV. Material coherence function," in *Infrared Spaceborne Remote Sensing 2005*, M. Strojnik, ed., Proc. SPIE 5883, Bellingham, 58830X (2005).
9. P. Vacas-Jacques, M. Strojnik, G. Paez, "Reduced coherence and calibration optimization for transillumination interferometry," in *Coherence Domain Optical Methods and Optical Coherence Tomography in Biomedicine XI*, J. Fujimoto, J. Izatt, V. Tuchin, eds., Proc. SPIE 6429, Bellingham, 64292K (2007).
10. P. Vacas-Jacques, M. Strojnik, G. Paez, "Monte-Carlo simulation of photon trans-illumination time of flight," in *Novel Optical Instrumentation for Biomedical Applications III*, C. Depeursinge, ed., Proc. SPIE 6631, Bellingham, 663114 (2007).
11. P. Vacas-Jacques, M. Strojnik, G. Paez, "Optimal source bandwidth for pass-through photon-based trans-illumination interferometry," in *Coherence Domain Optical Methods and Optical Coherence Tomography in Biomedicine XII*, J. Fujimoto, J. Izatt, V. Tuchin, eds., Proc. SPIE 6847, Bellingham, 68472S (2008).
12. P. Vacas-Jacques, G. Paez, M. Strojnik, "Pass-through photon-based biomedical transillumination," *J. Biomed. Opt.* **13**, 041307 (2008).
13. P. Vacas-Jacques, M. Strojnik, G. Paez, "Forward-calculated analytical interferograms in pass-through photon-based biomedical transillumination," *J. Opt. Soc. Am. A* **26**, 602–612 (2009).
14. Y. Pan, R. Birngruber, J. Rosperich, R. Engelhardt, "Low-coherence optical tomography in turbid tissue: Theoretical analysis," *Appl. Opt.* **34**, 6564–6574 (1995).
15. G. Xiong, P. Xue, J. Wu, Q. Miao, R. Wang, L. Ji, "Particle-fixed Monte Carlo model for optical coherence tomography," *Opt. Exp.* **13**, 2182–2195 (2005).
16. L. Wang, S. Jacques, L. Zheng, "MCML — Monte Carlo modeling of light transport in multi-layered tissues," *Comput. Meth. Progr. Biomed.* **47**, 131–146 (1995).
17. M. Yip, M. Carvalho, "A Monte-Carlo maplet for the study of the optical properties of biological tissues," *Comput. Phys. Commun.* **177**, 965–975 (2007).
18. R Development Core Team, *R: A Language and Environment for Statistical Computing*, R Foundation for Statistical Computing, Vienna (2009).
19. H. van Staveren, C. Moes, J. van Marle, S. Prahl, M. van Gemert, "Light scattering in Intralipid-10% in the wavelength range of 400–1100 nm," *Appl. Opt.* **30**, 4507–4514 (1991).
20. B. Devaraj, K. Fukuchi, K. Chan, M. Usa, Y. Tanno, M. Takeda, M. Kobayashi, H. Inaba, "Spectroscopic measurement of transmission characteristics of tissue-like phantoms," in *CLEO/Pacific Rim '95 Tech. Dig. Ser.*, OSA, Washington, pp. 126–127 (1995).

21. C. Bühler, P. Ngaotheppitak, D. Fried, "Imaging of occlusal dental caries (decay) with near-IR light at 1310 nm," *Opt. Exp.* **13**, 573–582 (2005).
22. D. Fried, J. Featherstone, C. Darling, R. Jones, P. Ngaotheppitak, C. Bühler, "Early caries imaging and monitoring with near-infrared light," *Dent. Clin. N. Am.* **49**, 771–793 (2005).
23. M. Polyanskiy, Refractive index database, http://refractiveindex.info.
24. G. Hale, M. Querry, "Optical constants of water in the 200-nm to 200-μm wavelength region," *Appl. Opt.* **12**, 555–563 (1973).
25. B. Pogue, M. Patterson, "Review of tissue simulating phantoms for optical spectroscopy, imaging and dosimetry," *J. Biomed. Opt.* **11**, 041102 (2006).